28. D. B. Nash and F. P. Fanale, *Icarus* **31**, 40 (1977).
29. I. Kupo *et al.*, *Astrophys. J.* **205**, L51 (1976).
30. A. L. Broadfoot *et al.*, *Science* **204**, 979 (1979).
31. R. L. Nelson and B. W. Hapke, *Icarus* **36**, 304 (1978).
32. C. B. Pilcher, S. T. Ridgway, T. B. McCord, *Science* **178**, 1087 (1972).
33. F. P. Fanale *et al.*, in *Planetary Satellites*, J. A. Burns, Ed. (Univ. of Arizona Press, Tucson, 1977), p. 379.
34. G. J. Consolmagno and J. S. Lewis, in *ibid.*, p. 492.
35. R. T. Reynolds and P. M. Cassen, *Geophys. Res. Lett.* **6**, 121 (1979).
36. T. V. Johnson and T. R. McGetchin, *Icarus* **18**, 612 (1973).
37. L. A. Lebofsky, *Nature (London)* **269**, 785 (1977); J. V. Pollack *et al.*, *Icarus* **36**, 271 (1978).
38. J. F. McCauley, *Phys. Earth Planet Interiors* **15**, 220 (1977).
39. D. Morrison, D. P. Cruikshank, J. A. Burns, in *Planetary Satellites*, J. A. Burns, Ed. (Univ. of Arizona Press, Tucson, 1977), p. 12.
40. P. H. Smith, *Icarus* **35**, 169 (1978).
41. J. D. Anderson, G. W. Null, S. K. Wong, *J. Geophys. Res.* **79**, 3361 (1974).
42. The success of this experiment has in a very real sense resulted directly from the individual contributions of several hundred men and women. Among these are the following: G. Bailey, H. T. Enmark, R. F. Lockhart, L. L. Simmons, and F. E. Vescelus (camera engineering); C. C. Avis, G. W. Garneau, P. L. Jepsen, J. J. Lorre, J. A. Mosher, D. J. Royer, A. A. Schwartz, M. J. Sullivan, G. M. Yagi, and the personnel of JPL's Mission Imaging Operations Group (data processing); R. Batson, P. Bridges, J. Inge, C. Isbell, B. K. Luchitta, G. G. Schaber, and R. Tyner (analysis and cartography); J. L. Anderson, R. P. Laeser, A. L. Lane, M. J. Sander, and C. H. Stembridge (project leadership); R. Gurrola, J. T. Harwood, R. Krauss, V. J. Nelson, L. Pieri, F. Popescu, and JPL's Photolab (supporting efforts); and especially M. L. Brownell, C. J. Hansen, P. N. Kupferman, J. L. Mitchell, and the Voyager Sequence Team for their skilled and tireless efforts to coax such magnificent data from a complicated and sometimes reluctant spacecraft. G. E. Hunt is supported by the Science Research Council, Great Britain. This report presents the results of one phase of research carried out at JPL under NASA contract NAS 7-100. We are grateful for careful reviews of the manuscript by M. Malin, D. Muhleman, J. Pearl, and R. Terrile.

17 April 1979

Discovery of Currently Active Extraterrestrial Volcanism

Abstract. *Two volcanic plumes were discovered on an image of Io taken as part of the Voyager optical navigation effort. This is the first evidence of active volcanism on any body in the solar system other than Earth.*

A photograph of Io (Fig. 1) taken by Voyager 1 revealed the first evidence of currently active volcanism on any solar system object other than Earth. This image was taken at 13:28 Greenwich mean time on 8 March 1979 from a range of 4.5×10^6 km. Io was photographed at this time as part of the Voyager optical navigation effort, a program to determine both the ephemerides of the five inner Jovian satellites and the trajectory of the spacecraft through the acquisition and analysis of satellite and star images.

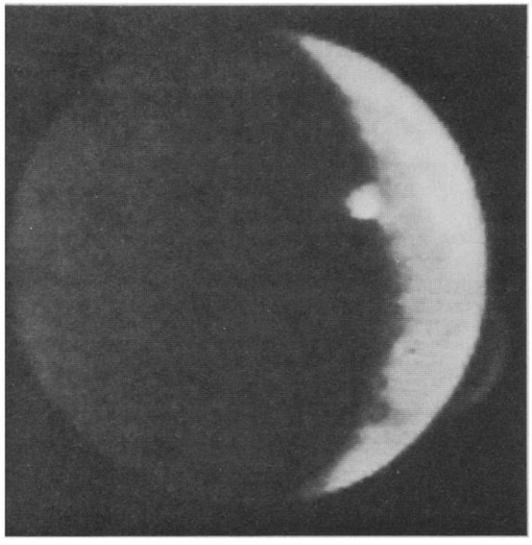

Fig. 1. Narrow-angle image of Io. This 0.96-second exposure was taken through a clear filter by Voyager 1, 3 days after the spacecraft's closest approach to Jupiter. The phase angle is 124°. The image has been digitally enhanced, in contrast and size, to more clearly show the faint cloud above Io's limb. Io's lit crescent is shown as well as its dark hemisphere, which is faintly illuminated by sunlight reflected by Jupiter. Two examples of volcanic plumes are found in this image.

Although not shown in Fig. 1, the original image includes two stars (AGK3-10021 and AGK3-20006). It was the digital processing used to display these faint stars that first revealed a dim cloud (< 10 percent of Io's brightness), which is apparent in the image as a thin crescent above the satellite's eastern limb. It appeared that this crescent might be a second solid body located beyond Io. However, this possibility was ruled out on two bases. First, the diameter of such an object would be sufficient—1000 km or greater—that it should have been previously detected, and second, the spacecraft was about 3° above the orbital plane of the Galilean satellites, so that none of these large bodies could have appeared in line with Io.

A more plausible interpretation of the image is that sunlight is being forward-scattered by a large, well-defined cloud of gas or dust located at least 270 km above the surface of Io. Considering the landforms observed on Io during the closest approach, this cloud is probably of volcanic origin. The cloud is located above, or nearly above, a heart-shaped feature on Io that has been independently identified as a volcanic landform. This feature, at 250° longitude, −30° latitude, can be located on figures 14 and 16 of (*1*), which contains additional examples and a discussion of Io volcanism. Subsequent analysis of this image has revealed that the bright spot at 305°, 10° (just beyond Io's terminator) is a second volcanic plume [see figure 19 in (*1*)] projecting above the dark surface into the sunlight.

L. A. Morabito
S. P. Synnott
P. N. Kupferman
Stewart A. Collins
Jet Propulsion Laboratory, California Institute of Technology, Pasadena 91103

References and Notes

1. B. A. Smith *et al.*, *Science* **204**, 951 (1979).
2. This report presents the results of one phase of research carried out at the Jet Propulsion Laboratory under NASA contract NAS 7-100.

25 April 1979

Infrared Observations of the Jovian System from Voyager 1

Abstract. *The infrared spectroscopy and radiometry investigation has obtained spectra of Jupiter and its satellites between approximately 180 and 2500 cm^{-1} with a spectral resolution of 4.3 cm^{-1}. The Jupiter spectra show clear evidence of H_2, CH_4, C_2H_2, C_2H_6, CH_3D, NH_3, PH_3, H_2O, and GeH_4. A helium concentration of 0.11 ± 0.03 by volume is obtained. Meridional temperature cross sections show considerable structure. At high latitudes, the stratosphere is warmer in the north than in the south. The upper troposphere and lower stratosphere are locally cold over the Great Red Spot. Amalthea is warmer than expected. Considerable thermal structure is observed on Io, including a relatively hot region in the vicinity of a volcanic feature.*

The Voyager infrared spectroscopy and radiometry investigation uses a Michelson interferometer operating in the infrared and a single-channel radiometer sensitive to visible radiation, both of which share a 50-cm Cassegrain telescope. This instrument, designated by the acronym IRIS (*1*), performed well during the Jupiter encounter, with more than 50,000 spectra recorded. Because of a small misalignment that developed during cruise between Earth and Jupiter, satisfactory responsivity of the interferometer is limited to the region be-

0036-8075/79/0601-0972$00.50/0

tween approximately 180 and 2500 cm^{-1} (4 and 55 μm). The average noise equivalent radiance for an individual spectrum falls steeply from 3×10^{-8} at 180 cm^{-1} to a minimum of 4×10^{-9} at 400 cm^{-1}; thereafter, it rises nearly linearly to 1.2×10^{-8} W-cm^{-2}-$ster^{-1}$/cm^{-1} at 2000 cm^{-1}.

Calibration of the absolute radiance level in the spectrometer was established by scaling the planetary and satellite spectra to deep space spectra, making use of a precise knowledge of the temperature of the instrument. The radiometer was calibrated by viewing solar radiation diffusely reflected from an onboard plate and specularly reflected from a small mirror mounted on the telescope. The resulting calibrated spectral and radiometer data are of good quality and allow many scientific objectives to be pursued, a few examples of which are discussed in this report.

Atmospheric composition. A large number of spectra of the Jovian atmosphere were acquired. The narrow field of view (0.25° full cone angle) permitted recording of full-disk spectra 3 to 4 weeks before closest approach with spatial resolution increasing to a maximum of almost 1/100 of the apparent disk diameter at closest approach.

The characteristics of the spectral region 180 to 1400 cm^{-1} are illustrated in Fig. 1 and those of the region 1700 to 2300 cm^{-1} in Fig. 2. For the low-wavenumber region examples are given for the North Equatorial Belt (NEB) under near-vertical viewing (emission angle ~ 9°) and limb viewing (~ 67°) conditions, and for the south polar region (~ 55°). For the high-wavenumber region, only spectra from the NEB are shown. A synthesized spectrum employing a representative belt temperature profile and composition information available from ground-based data (*2*) is also shown in Fig. 1.

The overall qualitative characteristics of the measured spectra compare favorably with the model, although noticeable quantitative differences exist. Evident spectral features include the high J rotation lines of NH_3 near 200 cm^{-1}, the broad pressure-induced translation-rotation $S(0)$ and $S(1)$ transitions of H_2 between 300 and 700 cm^{-1}, the ν_5 C_2H_2 rotation-vibration band centered at 729 cm^{-1}, the ν_2 NH_3 rotation-vibration band between 800 and 1200 cm^{-1}, and the ν_4 CH_4 rotation-vibration band between 1200 and 1400 cm^{-1}. The ν_9 band of C_2H_6 is easily identified in the high air mass spectra. The C_2H_2, C_2H_6, and central portions of the CH_4 band appear in emission, indicating their formation in the

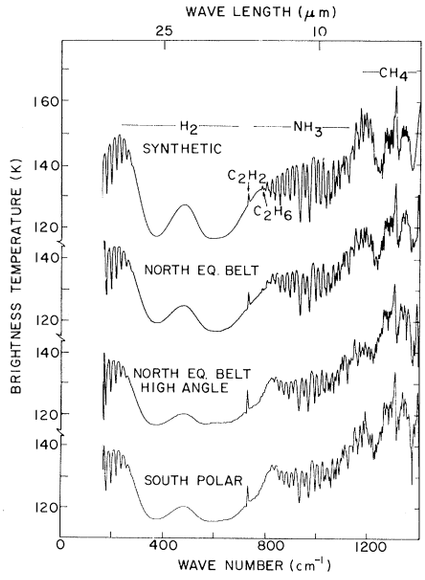

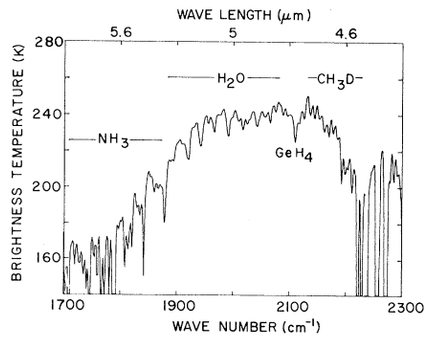

Fig. 1 (left). Observed thermal emission spectra for several locations over the Jovian disk. The spectral features observed for the gases H_2 and NH_3 are of tropospheric origin, and C_2H_2 and C_2H_6 are concentrated in the stratosphere. Methane is well mixed throughout both regions. The enhancement of the emission of the stratospheric species with air mass may be seen in the lowest two (high viewing angle) spectra. Fig. 2 (right). Thermal emission spectrum for the NEB in the Jovian 2000 cm^{-1} atmospheric window. Infrared radiation in this region originates from the deep atmosphere below the upper cloud deck. This spectrum is an average of 81 individual spectra.

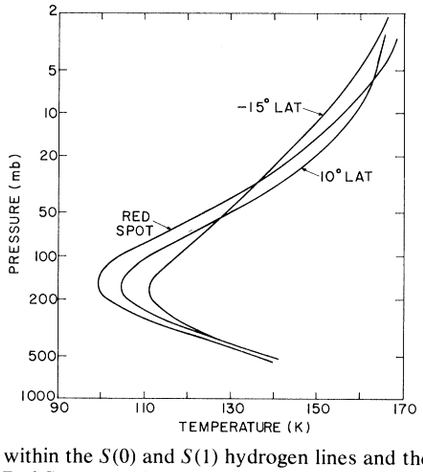

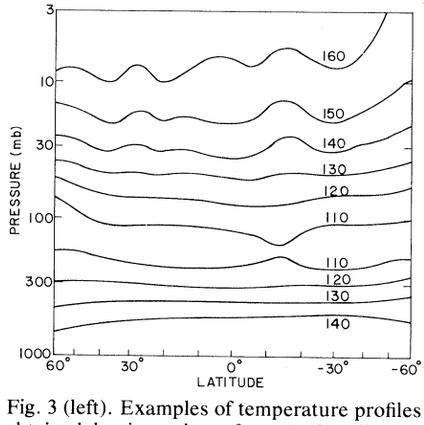

Fig. 3 (left). Examples of temperature profiles obtained by inversion of spectral radiances within the $S(0)$ and $S(1)$ hydrogen lines and the ν_4 band of methane. The profile over the Great Red Spot was obtained from an average of six spectra; those at +10° and −15° latitude are from averages of approximately 60 spectra. Fig. 4 (right). Zonally averaged meridional temperature cross section of Jupiter. Data from two global maps taken respectively 2 days before and 2 days after encounter were combined to obtain this result.

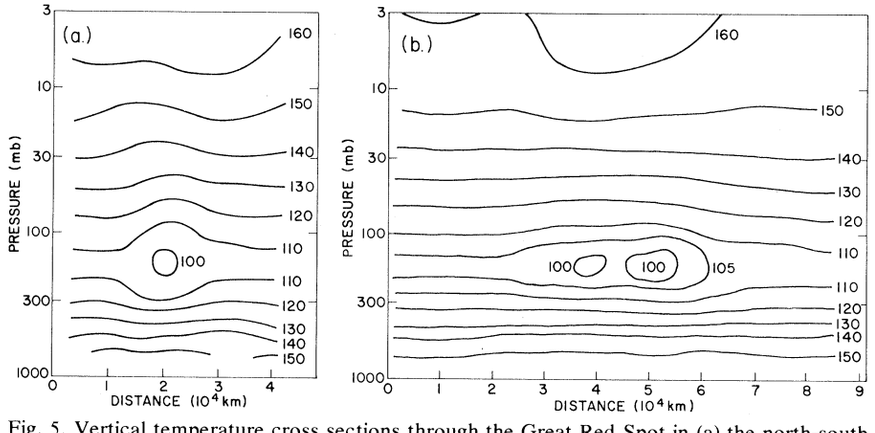

Fig. 5. Vertical temperature cross sections through the Great Red Spot in (a) the north-south direction and (b) the east-west direction. Each cross section is approximately centered on the spot.

stratosphere. The strength of the C_2H_2 and C_2H_6 features is found to change differentially with latitude, indicating corresponding differences in concentration or vertical distribution.

Small spectral features with temperatures ~ 0.3 K warmer than the surrounding continuum are observed at 354.4 and 587.1 cm^{-1}, the frequencies of the $S(0)$ and $S(1)$ lines of the free H_2 molecule. These features may be due to some combination of the quadrupole component of absorption (*3*) and intercollisional interference effects similar to those observed in the S lines in the fundamental vibration-rotation band (*4*). Significant PH_3 absorption between 1100 and 1200 cm^{-1} is seen, with the strongest spectral features not masked by NH_3 being the 1122 cm^{-1} Q branch and an R branch line at 1184 cm^{-1}.

The 2000 cm^{-1} region is transparent to the dominant Jovian gaseous absorbers H_2, CH_4, NH_3, and PH_3 and, in the absence of dense clouds, allows infrared radiation from the deeper atmosphere to emerge. Ground-based measurements in this spectral window show brightness temperatures that vary between 195 and 260 K, with strong radiation associated with localized hot spots where the intensity of the radiation increases with increasing spatial resolution (*5*). At a resolution of 1/20 of the disk, a temperature of 250 K was first seen from the spacecraft; at higher spatial resolution temperatures never exceeded 260 K, indicating a distinct lower boundary. The nature of this boundary is not clear; however, it could be either a cloud deck or a molecular absorption continuum.

The data shown in Fig. 2 were recorded at +12° latitude at 1/20 disk resolution. The region 1700 to 1900 cm^{-1} is dominated by the ν_4 NH_3 band with the continuum from this band apparently extending to 2000 cm^{-1}. Most of the strong absorption lines between 1900 and 2100 cm^{-1} are due to H_2O. The Q branch of GeH_4 at 2111 cm^{-1} and CH_3D absorption between 2100 and 2210 cm^{-1} are visible, in agreement with ground-based measurements (*6*).

Although preliminary, an attempt has been made to place limits on the He abundance. The He concentration was derived by using the method of Gautier and Grossman (*7*). This method takes advantage of the fact that the coefficients of H_2-H_2 and H_2-He collision-induced absorption vary differentially with wavenumber in the low-frequency portion of the spectrum. The H_2 and He opacities used were based on recent experimental and theoretical work (*8*). A systematic error in the He determination can occur if an additional unknown absorber is present at wavenumbers used for inverting the radiative transfer equation. To minimize the possibility of such a perturbation by clouds or haze or by the far wings of NH_3 lines, spectra were selected from belts, since these regions appear to be more highly transparent in the infrared than other locations on the planet. A total of 58 spectra were chosen for which the average brightness temperatures between 2000 and 2050 cm^{-1} exceeded 240 K and the brightness temperatures at 280 cm^{-1} and in the NH_3 continuum at 226 cm^{-1} exceeded 140 and 149 K, respectively. The wavenumbers chosen for the inversion in the H_2-He absorption range were 280, 310, 340, and 602 cm^{-1}. The volume fraction of He in the Jovian atmosphere is found to be 0.11, with a formal error of ± 0.03, which can be compared to the previous estimate of 0.12 ± 0.06 by Orton and Ingersoll (*9*).

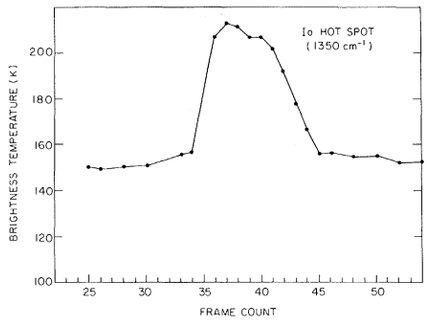

Fig. 6. Brightness temperature at 1350 cm^{-1} in the vicinity of a large hot spot on Io; the apparent 150 K background represents the instrument noise level at this wavenumber. In this representation, the width of the IRIS field of view corresponds to roughly seven frame counts. Frames 35 through 44 include portions of the central features in Fig. 7. The missing frame (number 35) was rejected during preliminary processing because of data errors, but is recoverable.

Thermal structure and dynamics. Vertical temperature profiles have been obtained by inversion of the radiative transfer equation, using measurements at selected frequencies within the $S(0)$ and $S(1)$ hydrogen lines and in the 1306 cm^{-1} methane band. Unresolved problems exist with the simultaneous fitting of all parts of the hydrogen lines; therefore, the retrievals presented here must be regarded as preliminary. However, certain gross features of the atmospheric thermal structure are worth noting at this time. Strong spatial variability is illustrated by the three profiles in Fig. 3. In all cases the lapse rate appears to be approximately adiabatic in the region below about 300 mbar, but substantial variations exist in the upper troposphere, at the tropopause, and in the stratosphere. The results appear to be generally consistent with those obtained from the Pioneer infrared data (*9*).

By combining selected sets of individual profiles, it is possible to investigate spatial gradients on both global and local scales. As a first effort to examine the global scale atmospheric thermal structure, zonally averaged meridional cross sections have been constructed from data acquired during two sequences in which the entire planet was mapped over 10-hour periods, using successive north-south scans. The two sets of data were combined to produce the cross section shown in Fig. 4. The troposphere is found to have relatively flat isotherms except at high latitudes; however, these deviations may be artifacts, since pointing uncertainties make the high-latitude footprint locations uncertain. The clouds associated with the zones appear to produce only small effects on the temperature profiles. For example, close inspection of the data indicates a depression of only ~ 2 K in inferred temperature at the 500-mbar level over the North Tropical Zone compared to the adjacent NEB. Spectra for this zone show brightness temperatures above 140 K in the continuum between the far-infrared rotation lines of NH_3, indicating that any cloud deck that is opaque in this spectral region must lie below ~ 600 mbar. However, semitransparent clouds and hazes at higher levels cannot be ruled out. The tropopause is found to be warmest and lowest at approximately −15° latitude, becoming cooler and higher at high latitudes. Direct deposition of solar energy into a stable lower stratosphere over a well-mixed troposphere without horizontal gradients would be expected to result in an equator-to-pole temperature decrease and tropopause height increase; however, the reason for the displacement of the maximum to the south is not apparent. The upper stratosphere is, on the average, cooler at high southern latitudes than at high northern latitudes, in agreement with previous ground-based observations (*10*). Such structure suggests a pole-to-pole meridional circulation of the upper stratosphere similar to the behavior of the terrestrial mesosphere. The strong latitudinal structure in the stratosphere was unanticipated, but appears to be a real phenomenon, substantially above the noise level of the measurements.

The only local dynamic phenomenon thus far examined is the Great Red Spot. Data have been analyzed from a sequence taken in the form of a cross centered on the spot, and temperature pro-

file retrievals have been combined to produce vertical cross sections through both the east-west and north-south axes of the spot, as shown in Fig. 5. The upper troposphere and lower stratosphere above the red spot are substantially colder than in the surrounding regions, with a maximum horizontal temperature difference at the tropopause of 5 to 7 K. Although the lower parts of the temperature profiles may be affected by clouds, brightness temperatures above 140 K are observed, again indicating that any opaque cloud deck lies below 600 mbar. Thermal winds have been estimated from the observed horizontal temperature gradients. With the assumption of a motionless state at 20 mbar, maximum wind velocities at 600 mbar are found to be approximately 75 m/sec in the east-west direction and 40 to 50 m/sec in the north-south direction, in rough agreement with the rotation period of approximately six Earth days observed by the imaging investigation. The observed anticyclonic motion of the spot implies a local pressure high, which, in the absence of a solid surface, requires a warm core. If such a warm region exists, it evidently lies below the levels accessible to the infrared measurements. The observed cold core is presumably associated with forced upward motion and vertically decaying tangential velocities of the spot. The penetration of the effects of the red spot into the stratosphere may possibly be understood within the framework of the vertical propagation of quasi-geostrophic disturbances (*11*). The stratosphere acts as a low-pass filter, permitting only long-wave components to propagate, while the shorter-wave components decay exponentially with a penetration depth of fL/N, where f is the Coriolis parameter ($\sim 10^{-4}$ sec^{-1}); N is the Brunt-Väisällä frequency, estimated from the stratospheric lapse rate to be $\sim 10^{-2}$ sec^{-1}; and L is the half-width of the spot ($\sim$ 5000 km). The resulting penetration depth of $\sim$ 50 km or two scale heights is in rough agreement with the penetration distance above the tropopause seen in Fig. 5. The larger-scale structure observed above 30 mbar may be longer-wave components that can propagate vertically.

Satellites. Satellites observed in the infrared include JI through JV. The few disk spectra of Amalthea indicate that the satellite is somewhat warmer than it would be if totally absorbing and heated only by Jupiter and the sun. This conflicts with the conclusion of Rieke (*12*). Possible sources of the additional energy are the Jovian radiation belt (*13*) and joule heating (*14*).

The thermal spectra of Europa, Ganymede, and Callisto are rather subdued, showing contrast differences on the order of 1 percent or less. Io, on the other hand, shows several features with contrast often exceeding 5 percent. This high contrast could result either from dust above the surface or from exposed bulk (nonpulverized) material. The spectral features have not yet been identified. Sulfur (S_8); such salts as sulfates, nitrates, and carbonates (*15, 16*); and various terrestrial volcanic products are among materials being investigated as possible sources of the spectral features on Io. In the reflected solar infrared (2000 to 3000 cm^{-1}), Io was marginally observed; the only feature evident above the noise is an absorption just below 2500 cm^{-1}, in agreement with observations made from Earth (*16*).

On Io, a large "hot spot" has been found in the IRIS data. The variation in brightness temperature at 1350 cm^{-1} as the instrument field of view crossed this region is shown in Fig. 6. Simultaneously obtained images show this to be associated with a clearly volcanic feature (Fig. 7) at approximately latitude $\lambda = +5°$, west longitude $\phi = 305°$, near which a plume originates (*17*). A thermal model in which some fraction b of the IRIS field of view is filled with hot (dark) material at a temperature T_1, and the remainder of the field is filled with a (light) background at a lower temperature T_2, seems consistent with the images. The thermal spectrum with such a model will be the sum of two blackbody functions whose relative weights are determined by the fraction b. Applying this model to the set of hot-spot spectra (Fig. 6) yields $b = 0.09 \pm 0.05$, $T_1 = 290 \pm 20$ K, and $T_2 = 127 \pm 2$ K. This at once rules out the possibility that all of the dark regions in Fig. 7 correspond to molten surfaces of any obvious candidate extrusive materials, such as silicates or even sulfur.

However, the inadequacy of the two-temperature model is also evident for the following reasons: the background temperature T_2 is somewhat below the expected surface solar equilibrium temperature of $\sim$ 135 K; the fits leave rather

Fig. 7. Narrow-angle imaging frame (FDSC 16 389:38) showing region of the hot spot on Io; material is being ejected from the nearly linear feature above the center of the picture. The diameter of the dark central region is about 200 km. The IRIS observations progressed generally from the lower left to the upper right. Estimates (see text) show that major portions of the dark regions near the center of the frame are significantly warmer than they would be if they were in equilibrium with solar radiation.

large residuals; and the variations in b and T_1 vary more from spectrum to spectrum than one might expect when looking at the displacements in the corresponding images. A more sophisticated model with several areas of different temperatures might be preferred; with such a model it may be possible to determine whether any areas with temperatures as high as the melting point of sulfur ($\sim$ 385 K) are present. Such refinements will also benefit both from better pointing information than is yet available and from recovery of the rejected IRIS frame indicated in Fig. 6. On a larger scale, the degree of correlation between volcanic landforms and hot areas remains to be determined.

The region just discussed represents the warmest area observed by the infrared experiment. Another type of thermal anomaly, in which temperature differentials on the order of 50 K exist over the instrument footprint, is very common, however. Arbitrarily considering these differentials to represent 50 K enhanced warm spots, such spots would often cover as much as 5 percent of the field. These areas might represent numerous local sources for expulsion of material, cooling extrusive material, or regions of subsurface activity. This type of anomaly is common over the portion of the planet on which the data are concentrated; based on preliminary pointing information, this is the region $-40° < \lambda < 30°$, $240° < \phi < 360°$. Very limited sampling in other regions, however, indicates that this is not planetwide; between latitudes $-20°$ and $-50°$, near longitudes 110° and 200°, such anomalies seem to be absent. It is apparent, however, that the IRIS observations on Io are consistent with observational (*18*) and theoretical (*19*) evidence for a thermally unusual and geologically active planet.

R. HANEL
B. CONRATH, M. FLASAR
V. KUNDE, P. LOWMAN
W. MAGUIRE, J. PEARL
J. PIRRAGLIA, R. SAMUELSON
Goddard Space Flight Center, Greenbelt, Maryland 20771
D. GAUTIER
Paris Observatory, Meudon, France
P. GIERASCH
Cornell University, Ithaca, New York 14853
S. KUMAR
Jet Propulsion Laboratory, Pasadena, California 91103
C. PONNAMPERUMA
University of Maryland, College Park 20742

References and Notes

1. R. Hanel *et al.*, *Space Sci. Rev.* **21**, 103 (1977).
2. R. G. Prinn and T. Owen, in *Jupiter*, T. Gehrels, Ed. (Univ. of Arizona Press, Tucson, 1976), p. 319; S. T. Ridgway, H. P. Larson, U. Fink, in *ibid.*, p. 384. The CH_4 volume mixing ratio adopted was 8.14×10^{-4}, based on the assumption of a solar C : H ratio.
3. D. Goorvitch and C. Chackerian, Jr., *Icarus* **32**, 348 (1977).
4. J. D. Poll, J. L. Hunt, J. W. Mactaggart, *Can. J. Phys.* **53**, 954 (1975).
5. R. J. Terrile and J. A. Westphal, *Icarus* **30**, 274 (1977): R. J. Terrile, thesis, California Institute of Technology, Pasadena (1978).
6. U. Fink, H. P. Larson, R. R. Treffers, *Icarus* **34**, 344 (1978); R. Beer and F. W. Taylor, *Astrophys. J.* **219**, 763 (1978); H. P. Larson, R. R. Treffers, U. Fink, *ibid.* **211**, 972 (1977); R. Beer and F. W. Taylor, *ibid.* **179**, 309 (1973); H. P. Larson, U. Fink, R. Treffers, T. N. Gautier III, *Astrophys. J. Lett.* **197**, L137 (1975).
7. D. Gautier and K. Grossman, *J. Atmos. Sci.* **29**, 788 (1972).
8. G. Birnbaum, *J. Quant. Spectrosc. Radiat. Transfer* **19**, 51 (1978); G. Birnbaum and E. R. Cohen, *Can. J. Phys.* **54**, 593 (1976).
9. G. S. Orton and A. P. Ingersoll, in *Jupiter*, T. Gehrels, Ed. (Univ. of Arizona Press, Tucson, 1976), p. 197.
10. W. Sinton, W. Macy, G. S. Orton, *Bull. Am. Astron. Soc.* **10**, 563 (Abstr.) (1978).
11. J. G. Charney and P. G. Drazin, *J. Geophys. Res.* **66**, 83 (1961).
12. G. H. Rieke, *Icarus* **25**, 333 (1975).
13. J. R. Thomas, *Eos* **53**, 1090 (1972).
14. N. F. Ness, M. H. Acuna, R. P. Lepping, L. F. Burlaga, K. W. Behannon, F. M. Neubauer, *Science* **204**, 982 (1979).
15. D. B. Nash and F. P. Fanale, *Icarus* **31**, 40 (1977); R. M. Nelson and B. W. Hapke, *ibid.* **36**, 304 (1978).
16. J. B. Pollack, F. C. Witteborn, E. F. Erickson, D. W. Strecker, B. J. Baldwin, T. E. Bunch, *ibid.* **36**, 271 (1978); D. P. Cruikshank, T. T. Jones, C. B. Pilcher, *Astrophys. J.* **225**, L89 (1978).
17. B. A. Smith *et al.*, *Science* **204**, 951 (1979).
18. O. L. Hansen, *Icarus* **18**, 237 (1973); F. C. Witteborn, J. D. Bregman, J. B. Pollack, *Science* **203**, 643 (1979).
19. S. J. Peale, P. Cassen, R. T. Reynolds, *Science* **203**, 892 (1979).
20. We thank D. Vanous, D. Crosby, and J. Taylor and their colleagues at Texas Instruments, Goddard Space Flight Center (GSFC), and Jet Propulsion Laboratory (JPL) for preparation of the instrumentation. L. Herath (GSFC), F. Rockwell, C. Otis, and R. Thompson (Astro Data Systems Inc.) contributed substantially to the data reduction. K. Fox provided molecular constants for methane. T. Burke, E. Miner, D. Collins, and L. Horn (JPL) made substantial contributions. We also thank the imaging team, especially B. Smith, G. Hunt, H. Masursky, and R. Terrile for many discussions, for permission to use Fig. 7, and for help in the selection of 5-μm hot spots for IRIS observations. The support of the Voyager Project Staff is also gratefully acknowledged. Portions of the research described in this report were supported by the Jet Propulsion Laboratory, California Institute of Technology, under NASA contract NAS 7-100.

20 April 1979

Radio Science with Voyager 1 at Jupiter: Preliminary Profiles of the Atmosphere and Ionosphere

Abstract. *A preliminary profile of the atmosphere of Jupiter in the South Equatorial Belt shows (i) the tropopause occurring at a pressure level of 100 millibars and temperature of about 113 K, (ii) a higher warm inversion layer at about the 35-millibar level, and (iii) a lower-altitude constant lapse rate matching the adiabatic value of about 2 K per kilometer, with the temperature reaching 150 K at the 600-millibar level. Preliminary afternoon and predawn ionospheric profiles at 12° south latitude and near the equator, respectively, have topside plasma scale heights of 590 kilometers changing to 960 kilometers above an altitude of 3500 kilometers for the dayside, and about 960 kilometers at all measured heights above the peak for the nightside. The higher value of scale height corresponds to a plasma temperature of 1100 K under the assumption of a plasma of protons and electrons in ambipolar diffusive equilibrium. The peak electron concentration in the upper ionosphere is approximately 2×10^5 per cubic centimeter for the dayside and about a factor of 10 less for the nightside. These peaks occur at altitudes of 1600 and 2300 kilometers, respectively. Continuing analyses are expected to extend and refine these results, and to be used to investigate other regions and phenomena.*

The planned radio science investigations with Voyager, the radio equipment parameters, and the mission characteristics of importance in these experiments have been described (*1*, *2*); we now present preliminary results on features of the atmosphere and ionosphere of Jupiter based on the occultation of Voyager 1 by the planet. During occultation, the radio rays from the spacecraft to Earth traverse these regions and the radio signal characteristics are affected in measurable ways. Because questions have been raised about the accuracy of such experiments, we also briefly describe several relevant aspects of the Voyager investigation.

Pioneer 10 and 11 were used in the first radio occultation experiments at Jupiter. The errors in early published atmospheric profiles based on these measurements (*3*) have resulted in concern that the occultation technique might never be useful for studying the neutral atmospheres of the giant planets. Although several key error sources were subsequently identified, and modified atmospheric profiles were published (*4*, *5*), appreciable uncertainties in these newer results still remain, and the doubts have not been wholly resolved.

The Voyager occultation experiment has several features that are expected to improve the accuracy and reliability of its final results. These include the use of (i) two coherent radio frequencies [wave-

0036-8075/79/0601-0976$00.50/0